Electronic Supplementary Material (ESI) for Physical Chemistry Chemical Physics.

Supporting Information for

Bi_2S_3 Nanorods Grown on Multiwalled Carbon Nanotubes as Highly Active Catalysts for CO_2 Electroreduction to Formate

Fangfang Yang[b], Zailai Xie[c], Xuke Huang[d], Xiangyang Yin[b], Weifeng Zhang[b], Yongkui Huang[e], Daijun Zhang[a,b*].

State Key Laboratory of Coal Mine Disaster Dynamics and Control, Chongqing University, Chongqing 400044, China.

Department of Environmental Science, Chongqing University, Chongqing 400044, China. E-mail: dzhang@cqu.edu.cn; Tel: 86-023-65105875.

Experimental sections

Electrocatalytic CO_2 Reduction

To prepare the working electrode, 3 mg materials and 1 mg ketjen black were suspended in a mixture of ethanol (360 μL, 95%), Nafion solution (40 μL, 5%), and ultrasonic treatment for 1 h. Then, 16 μL ink was dropped on the surface of the glass carbon electrode with an area of 0.196 cm^2 and dried at room temperature. Typically, the linear sweep voltammetry (LSV) curves were produced at a scan rate of 10 mV s^{-1}. All of the potentials were converted to the reversible hydrogen electrode E(*vs.*RHE) (V) = E(Ag/AgCl) + 0.2046 + 0.0591pH and corrected by iR drop compensation. The chronoamperometry tests were conducted at different potentials for 1 h. The electrochemical surface area (ECSA) was examined from 0.09 V to 0.19 V by cyclic voltammetry (CV). Electrochemical impedance spectroscopy (EIS) were measured from 100 000 Hz to 0.1 Hz at -0.76 V vs. RHE. All the measurements were conducted under ambient pressure at room temperature. The Faradaic efficiency (FE) towards formate (FE_{HCOO-}) is calculated by the equation:

$$FE = \frac{2nF}{Q} \times 100\% \quad (1)$$

Where *2* is the number electron transferred for $HCOO^-$, H_2 or CO, *n* is the mole of the product $HCOO^-$, *F* is Faraday constant (96,485), and *Q* is total electric charge integrated by *i-t* curve.

The Faradaic efficiency for the products of CO and H_2 (FE_{CO} *or* FE_{H2}) is calculated by the equation:

$$FE_{CO/H2} = \frac{10^{-3} mv\%FG}{60RTi} P \quad (2)$$

Where *v%* is the volume concentration of CO/H_2 in the collected gases from the headspace of the cell, *G* is flow rate of CO_2 bubbled into the cell (mL min^{-1}), *m* is the number of electrons transferred for the products CO and H_2 (here m=2), *i* is the current (mA), $P = 1.01\times10^5$ Pa, $R = 8.314$ J mol^{-1} K^{-1}, $T = 273.15$ K.

Theoretical Calculations

The present first principle DFT calculations are performed by Vienna Ab initio Simulation Package(VASP) [1] with the projector augmented wave (PAW) method[2]. The exchange-functional is treated using the generalized gradient approximation (GGA) of Perdew-Burke-Ernzerhof (PBE) functional.[3] The Spin-polarizations were carried out for all calculations. The energy cutoff for the plane wave basis expansion was set to 450 eV and the force on each atom less than 0.03 eV/Å was set for convergence criterion of geometry relaxation. The k-points in the Brillouin zone were sampled by a 2×2×1 grid. The self-consistent calculations apply a convergence energy

threshold of 10-5 eV. The DFT-D3 method was employed to consider the van der Waals interaction. [4] A 15 Å vacuum was added along the z direction in order to avoid the interaction between periodic structures. The free energies of the CO_2RR steps were calculated by the equation:[5]

$$\Delta G = \Delta E\_DFT + \Delta E\_ZPE - T\Delta S$$

where ΔEDFT is the DFT electronic energy difference of each step, ΔEZPE and ΔS are the correction of zero-point energy and the variation of entropy, respectively, which are obtained by vibration analysis, T is the temperature (T = 300K).

The CNTs model consists of 120 C atoms, and the Bi_2S_3-CNTs model loads a Bi_2S_3 isolated atomic cluster based on the CNTs model to represent the interface relationship of the composite structure. The Bi_2S_3 structure consists of 48 Bi atoms and 72 S atoms.

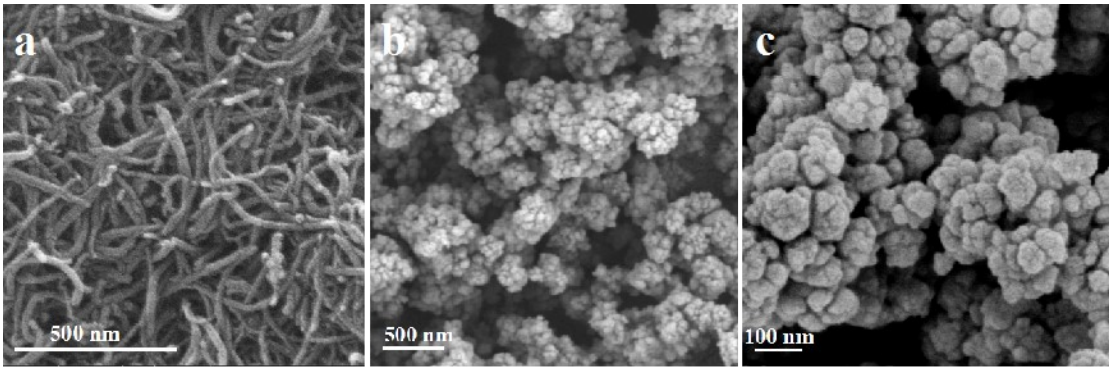

Fig. S1. SEM images of (a) CNTs, (b and c) pure Bi_2S_3 materials, respectively.

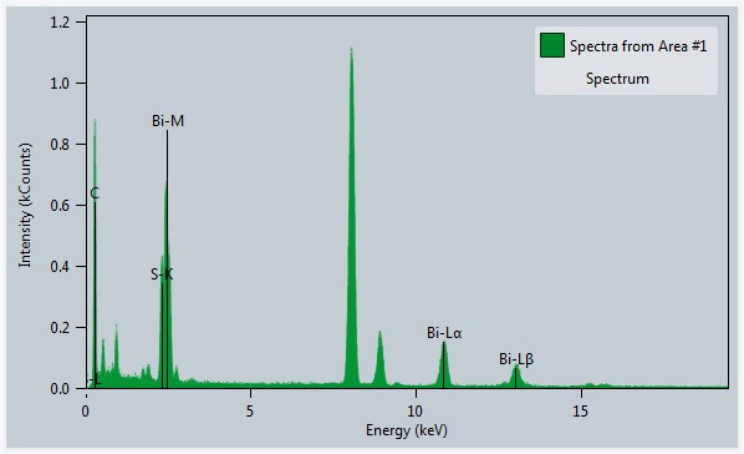

Fig. S2. EDS spectrum of Bi_2S_3/CNTs nanocomposite.

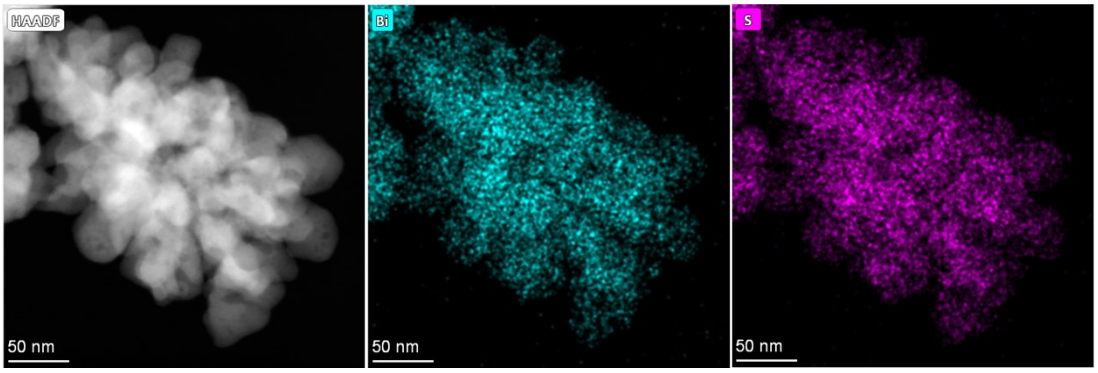

Fig. S3. TEM images and corresponding element mapping including Bi, S of Bi_2S_3 material.

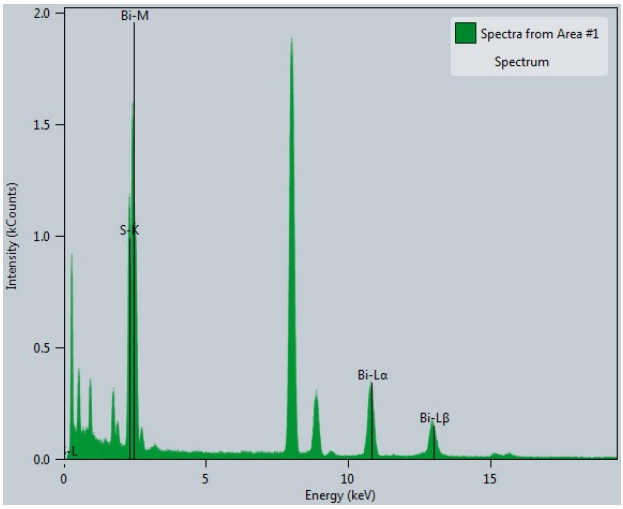

Fig. S4. EDS spectrum of pure Bi_2S_3 material.

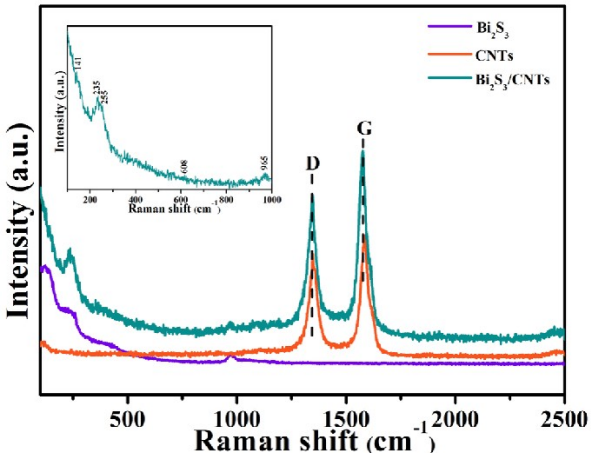

Fig. S5. Raman spectra of CNTs, Bi_2S_3, Bi_2S_3/CNTs materials.

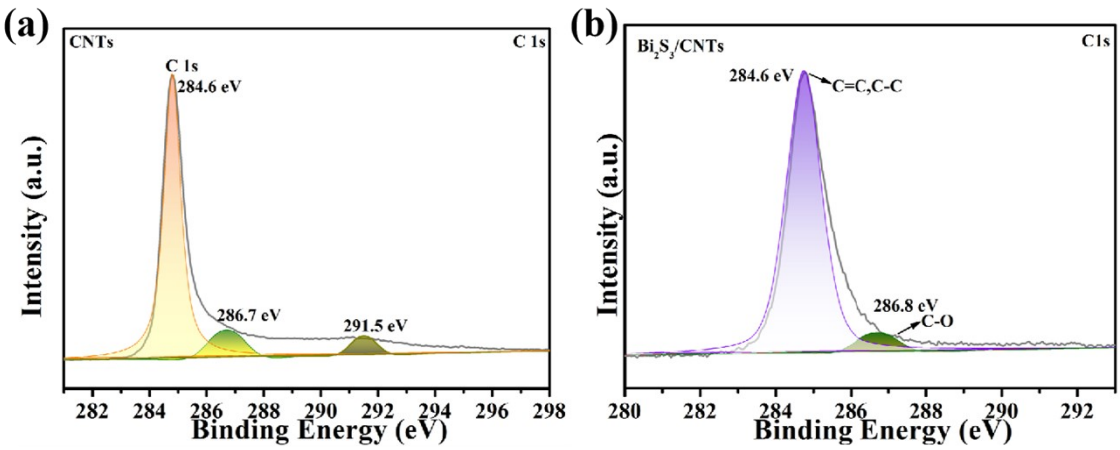

Fig. S6. X-ray photoelectron spectroscopy (XPS) survey of (a) CNTs and (b) Bi_2S_3/CNTs materials.

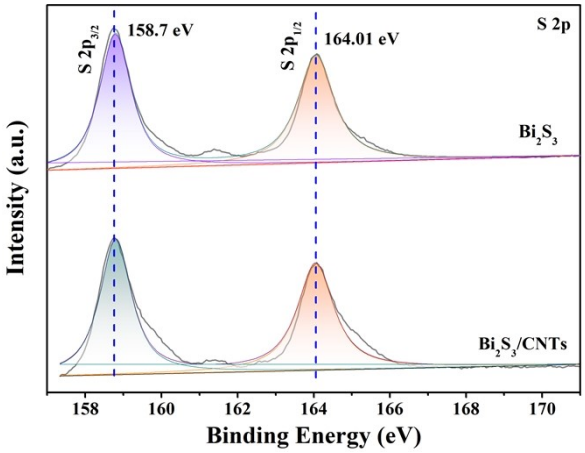

Fig. S7. S 2p spectra of Bi_2S_3, and Bi_2S_3/CNTs materials.

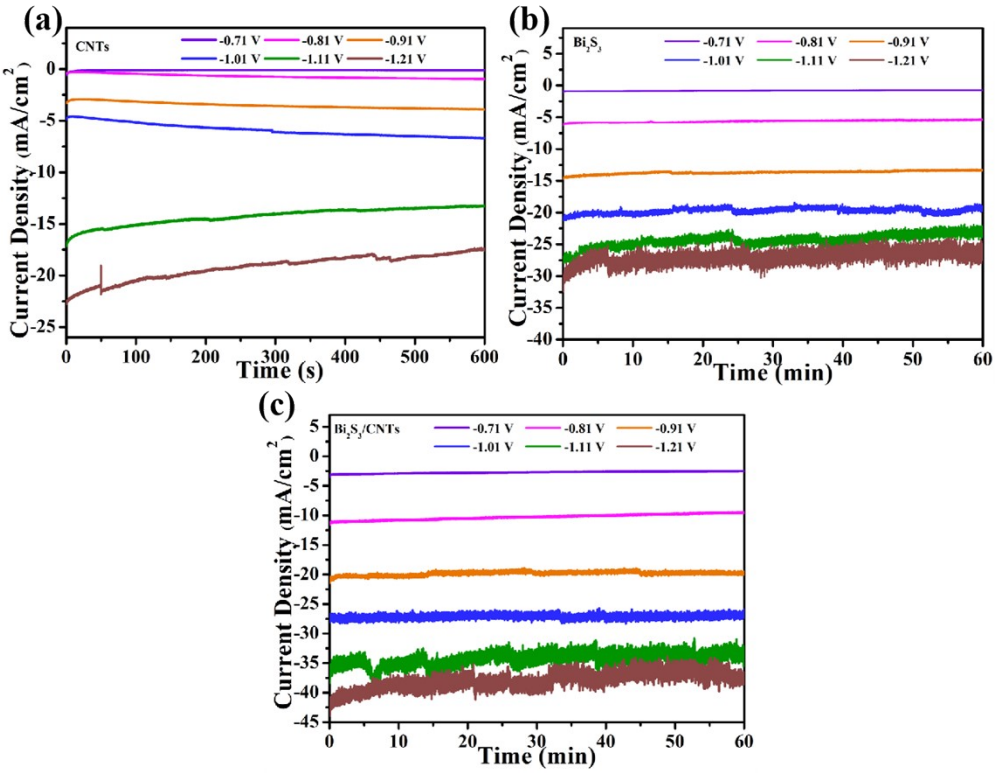

Fig. S8. Corresponding current density profile of the various catalysts at the selected potential for 60 min electrolysis: (a) CNTs, (b) Bi_2S_3, (c) Bi_2S_3/CNTs nanocomposite.

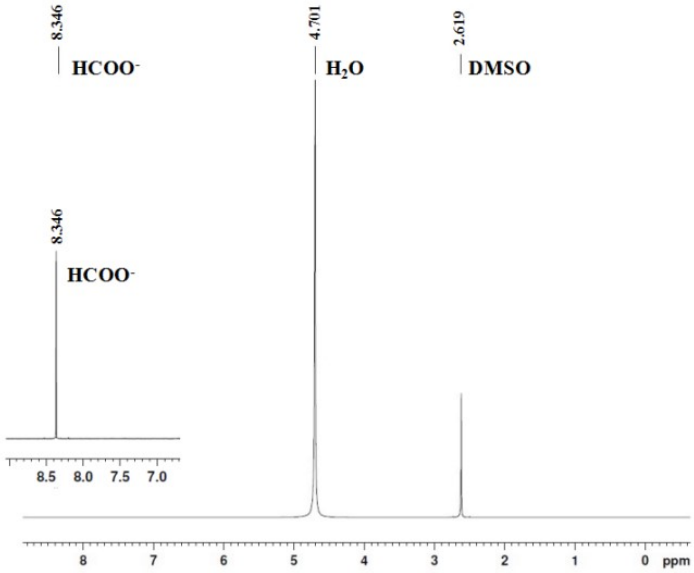

Fig. S9. The 1H NMR spectra of $KHCO_3$ electrolyte after electrolysis test over Bi_2S_3/CNTs catalyst.

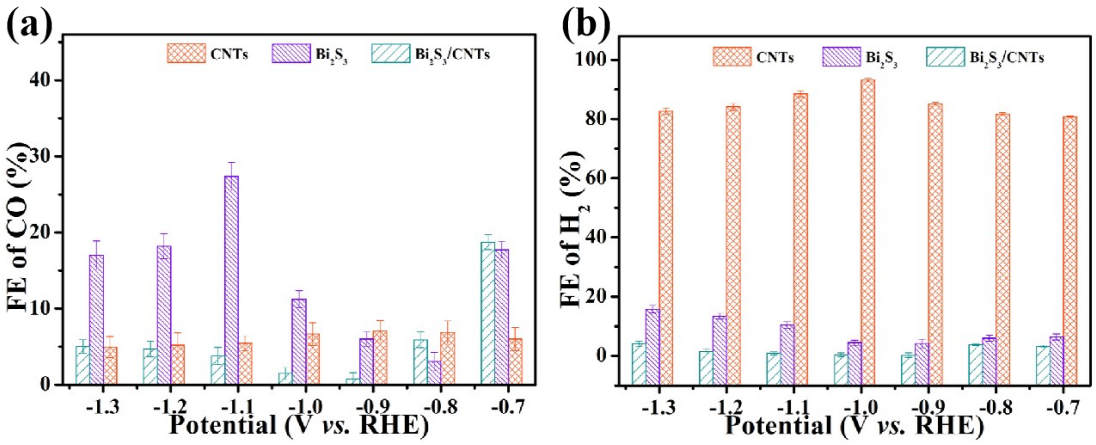

Fig. S10. FE of (a) CO and (b) H_2 of three catalysts at different potentials.

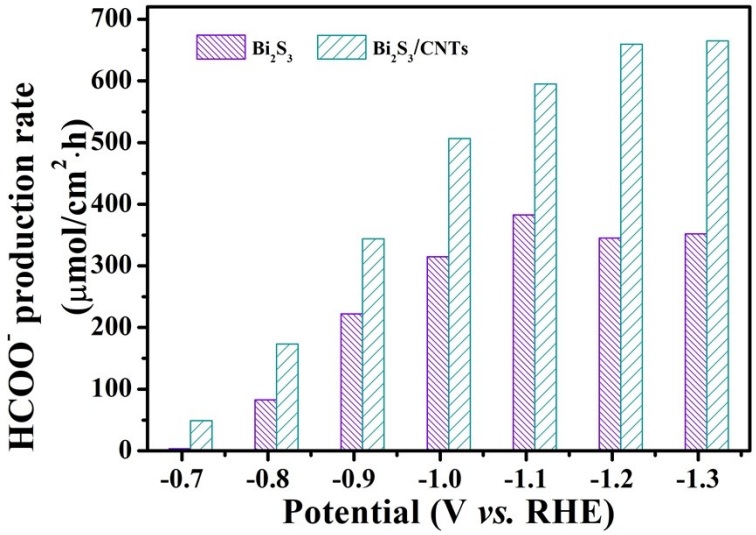

Fig. S11. $HCOO^-$ production rates of pure Bi_2S_3 and Bi_2S_3/CNTs nanocomposite at various potential for 60 min.

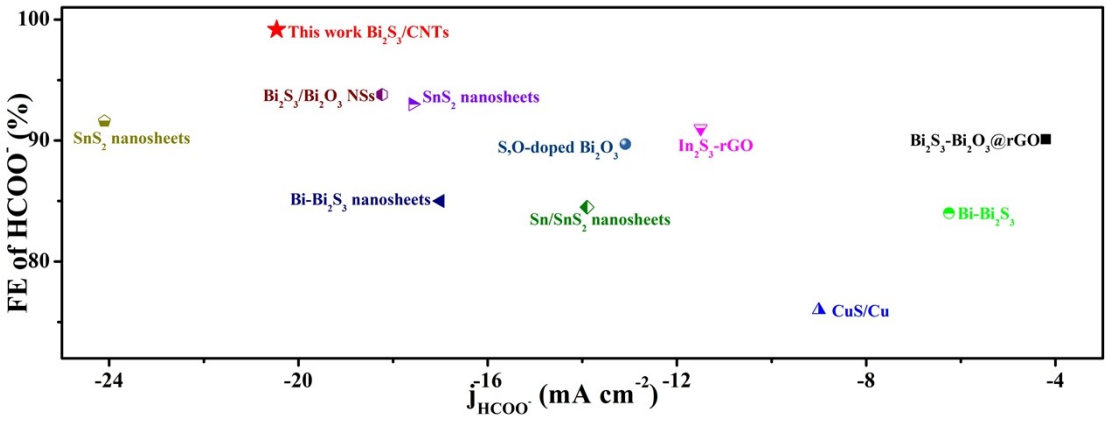

Fig. S12. Comparison of the electrocatalytic activity of our catalyst with other state-of-the-art catalysts for electrochemical reduction of CO_2 to $HCOO^-$.

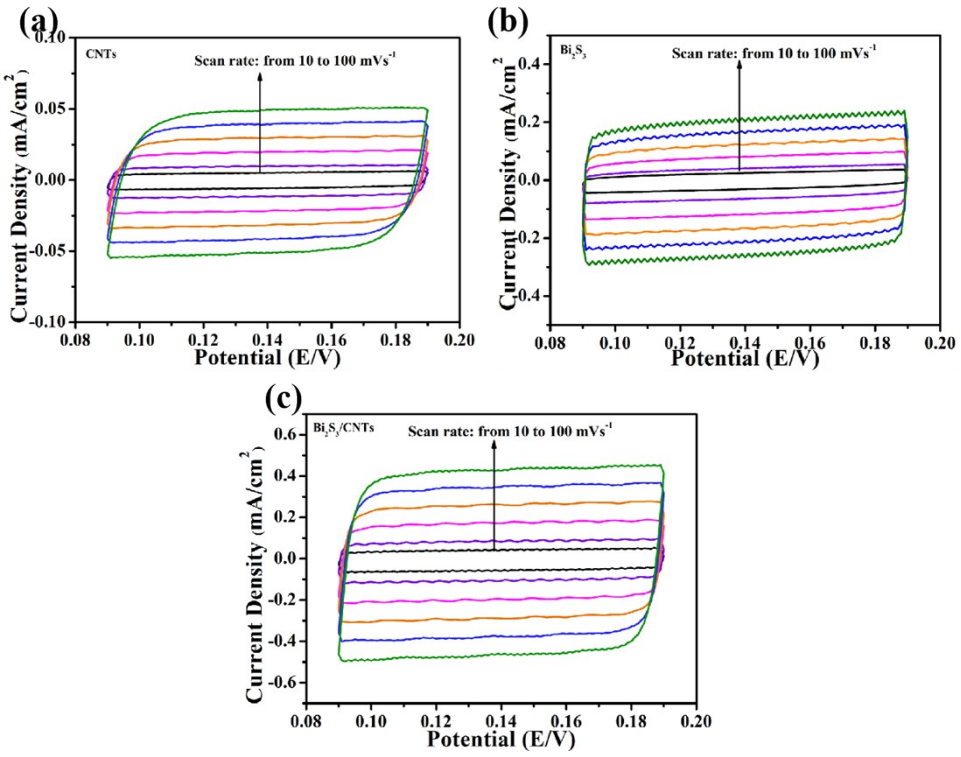

Fig. S13. CV curves at scan rates from 10 to 100 mV s^{-1}.

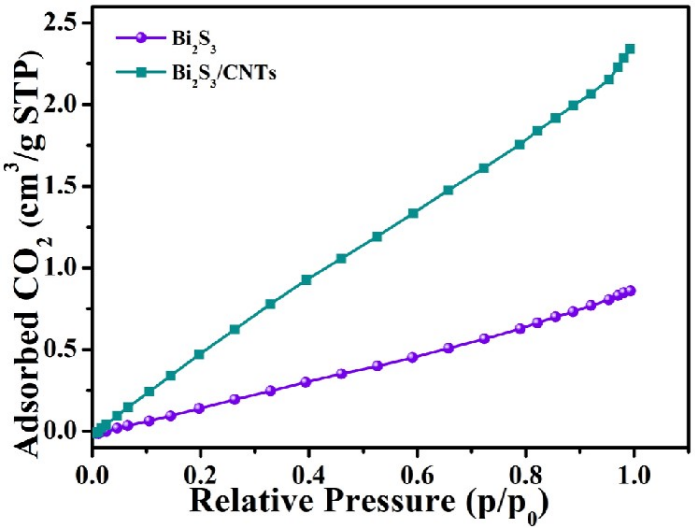

Fig. S14. CO_2 sorption isotherm of Bi_2S_3 and Bi_2S_3/CNTs, respectively.

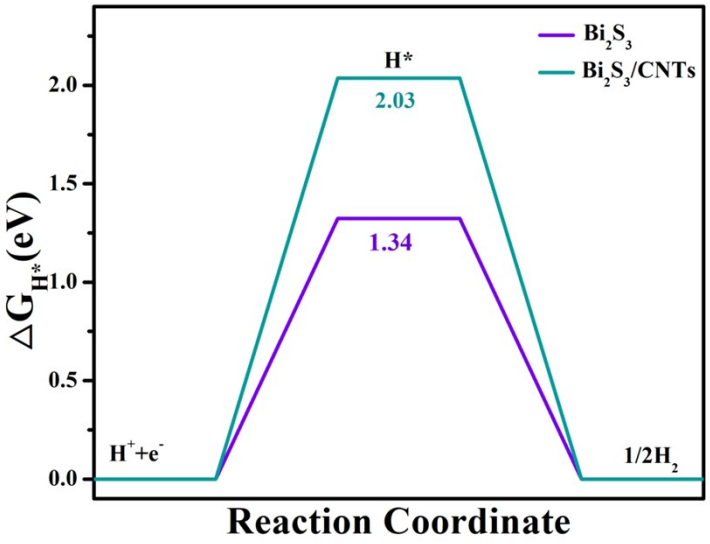

Fig. S15. Free-energy diagrams for H_2 formation on the Bi_2S_3 and Bi_2S_3/CNTs catalysts.

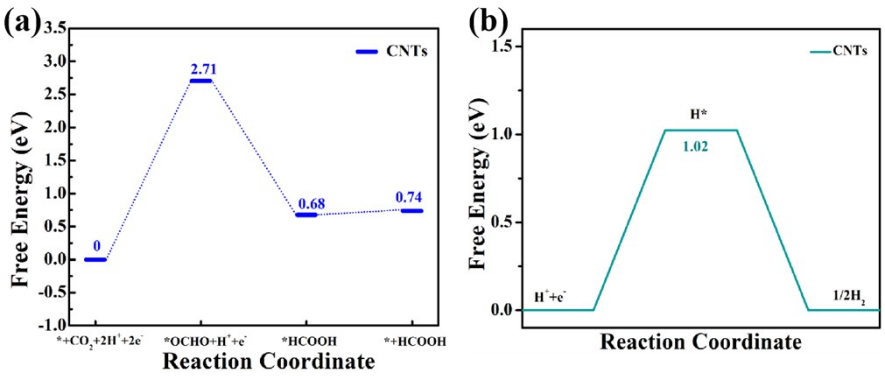

Fig. S16. Free-energy diagrams for formate and H_2 formation on the CNTs catalysts.

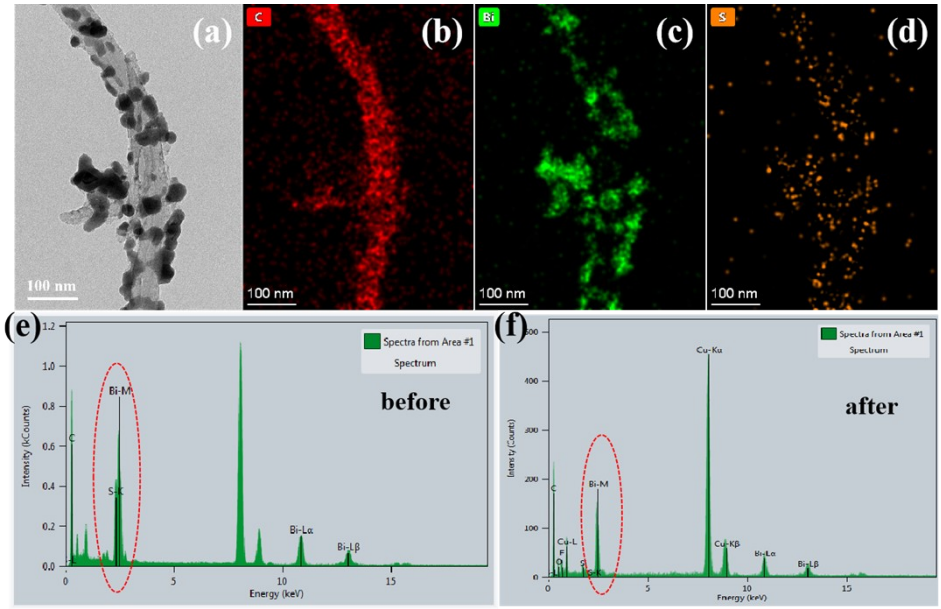

Fig. S17. (a) TEM, (b-d) elemental mapping of Bi_2S_3/CNTs after electrolysis, (e,f) EDS spectrum of Bi_2S_3/CNTs before and after electrolysis, respectively.

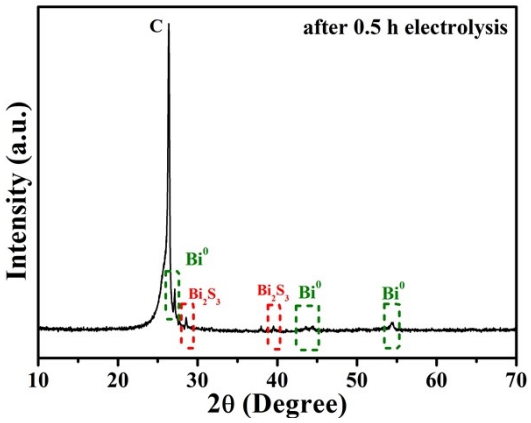

Fig. S18. XRD pattern of the Bi_2S_3/CNTs catalyst after 0.5 h electrolysis.

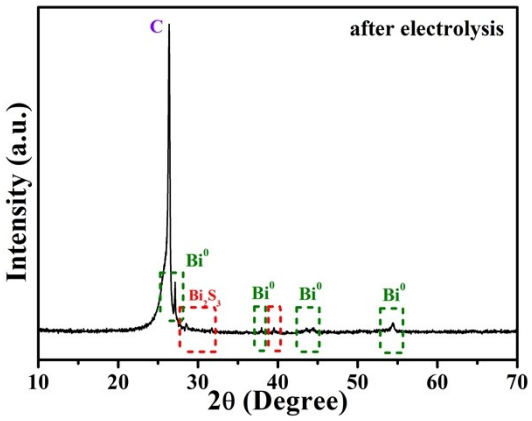

Fig. S19. XRD pattern of the Bi_2S_3/CNTs catalyst after long-time electrolysis.

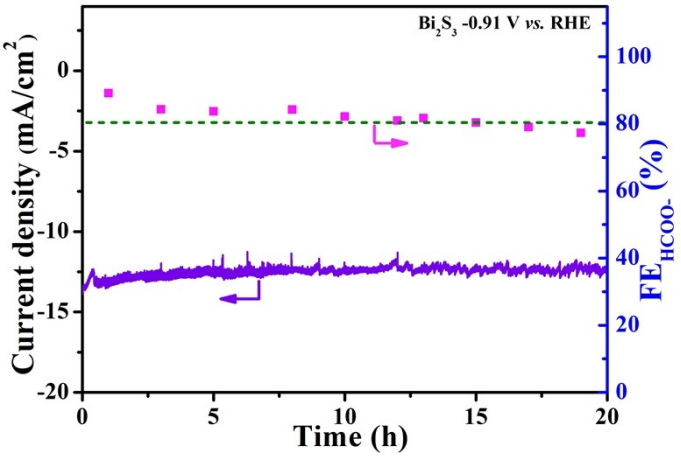

Fig. S20. Stability tests of Bi_2S_3 at electrolysis potentials of −0.91 V vs. RHE with current density and FE_{HCOO^-} at different times.

Table S1. Comparison of the electrocatalytic activity of our catalyst with other state-of-the-art catalysts for electrochemical reduction of CO_2 to $HCOO^-$ in aqueous media.

Electrocatalysts	Potential (V vs. RHE)	Electrolyte	FE_{HCOO^-} (%)	Reference	j (mA cm^{-2})
This work	**-0.91**	**0.5 M $KHCO_3$**	**99.3**		**-20.36**
In_2S_3-RGO composite	-1.2	0.1 M $KHCO_3$	91	6	-11.50
Bi-Bi_2S_3 nanosheets	-1.0	0.1 M $KHCO_3$	85	7	17.00
SnS_2 Nanosheets	-0.9	0.1 M $KHCO_3$	93	8	-17.58
Bi_2S_3-Bi_2O_3@rGO	-0.9	0.1 M $KHCO_3$	90.1	9	-4.20
SnS_2 nanosheets	-0.9	0.5 M $KHCO_3$	83.2	10	-24.10
Bi_2S_3-Bi_2O_3 NSs	-1.1	0.1 M $KHCO_3$	93.8	11	-18.23
Sn/SnS_2 nanosheets	-0.88	0.5 M $NaHCO_3$	84.5	12	-13.90
Bi-Bi_2S_3	-0.87	0.5 M $NaHCO_3$	84.0	13	-6.25
CuS/Cu	-0.9	0.1 M $KHCO_3$	75	14	-9.00
PbS	-1.2	0.1 M $KHCO_3$	97.6	15	-
S,O-doped Bi nanorods	-1.09	0.1 M $KHCO_3$	89.4	16	13.09

References

1. G. Kresse, Furthmüller, *J. Comp Mater Sci.,* 1996, **6**, 15.

2. P.E. Blöchl, *Phys. Rev. B,* 1994, **50**, 17953.

3. J.P. Perdew, J.A. Chevary, S.H. Vosko, K.A. Jackson, M.R. Pederson, D.J. Singh, *C.* Fiolhais, *Phys. Rev. B,* 1992, **46**, 6671.

4. S. Grimme, J. Antony, S. Ehrlich, H. Krieg, *J. Chem. Phys.* 2010, **132**, 154104.

5. E. Skulason, T. Bligaard, S. Gudmundsdottir, F. Studt, J. Rossmeisl, F. Abild-Pedersen, T. Vegge, H. Jonsson, J.K. Norskov, *Phys. Chem. Chem. Phys.,* 2012, **14**, 1235.

6. H. Ning, X. Fei, Z.H. Tan, W.H. Wang, Z.X. Yang, M.B. Wu, *ACS Appl. Nano Mater.* 2022, **5**, 2335-2342.

7. X.L. Shao, Y.Y. Liu, *J. Electrochem. Soc.,* 2022, **169**, 026505.

8. A. Zhang, Y.X. Liang, H.P. Li, S.L. Wang, Q.X. Chang, K.Y. Peng, Z.G. Geng, J. Zeng, *Nano Lett.,* 2021, **21**, 7789-7795.

9. X.X. Yang, P.L. Deng, D.Y. Liu, S. Zhao, D. Li, H. Wu, Y.M. Ma, B.Y. Xia, M.T. Li, C.H. Xiao, S.J. Ding, *J. Mater. Chem. A,* 2020, **8**, 2472-2480.

10. W. Zhang, W.K. Zhu, T. Yao, *Nano Micro Lett.,* 2021, **3**, 189.

11. P.F. Sui, C.Y. Xu, M.N. Zhu, S.B. Liu, Q.X. Liu, J.L. Luo, *Small,* 2022, **18**, 2105682.

12. F.W. Li, L. Chen, M.Q. Xue, T. Williams, Y. Zhang, D.R. MacFarlane, J. Zhang, *Nano Energy,* 2017, **31**, 270-277.

13. Y. Zhang, F.W. Li, X.L. Zhang, T. Williams, C.D. Easton, A.M. Bond, J. Zhang, *J. Mater. Chem. A,* 2018, **6**, 4714-4720.

14. Y. Deng, Y. Huang, D. Ren, A.D. Handoko, Z.W. Seh, P. Hirunsit, B.S. Yeo, *ACS Appl. Mater. Inter.,* 2018, **10**, 28572-28581.

15. J.W. Lim, W.J. Dong, J.Y. Park, D.M. Hong, J.L. Lee, *ACS Appl. Mater. Inter.,* 2020, **12**, 22891-22900.

16. X.L. Shao, X.L. Sun, Q. Huang, J. Yi, J.J. Zhang, Y.Y. Liu, *Dalton Trans.,* 2022, **51**, 7223-7233.